Mathware & Soft Computing 10 (2003) 155-168

Innovative Applications of Associative Morphological Memories for Image Processing and Pattern Recognition

M. Graña[1], P. Sussner[2], G. Ritter[3]
[1]Dept. CCIA, UPV/EHU, San Sebastian, Spain
ccpgrrom@si.ehu.es
[2] Institute of Math.,Stat. and Sci. Comp.
State University of Campinas, Brazil
[3] Center for Comp. Vision and Visual.
University of Florida

Abstract

Morphological Associative Memories have been proposed for some image denoising applications. They can be applied to other less restricted domains, like image retrieval and hyperspectral image unsupervised segmentation. In this paper we present these applications. In both cases the key idea is that Autoassociative Morphological Memories selective sensitivity to erosive and dilative noise can be applied to detect the morphological independence between patterns. Linear unmixing based on the sets of morphological independent patterns de¯ne a feature extraction process that is the basis for the image processing applications. We discuss some experimental results on the ¯sh shape data base and on a synthetic hyperspectral image, including the comparison with other linear feature extraction algorithms (ICA and CCA).

1 Introduction

Linear feature extraction algorithms, like Principal Component Analysis (PCA) [2], Linear Discriminant Analysis (LDA) [2], Independent Component Analysis (ICA) [7] are defined as a linear transformation that minimizes some criterion function, like the mean square error (PCA), a class separability criterion (LDA) or an independence criterion (ICA). The approach we take is to try to characterize the data by a convex region that encloses them or most of them. The features extracted are the relative coordinates of the data points in this region. In other words the result of the linear unmixing relative to the vertices of this convex region. Therefore the dimensionality reduction depends on the degree of detail of the definition of this convex region: the number of vertices that describe it. Depending on the application, the meaning of these vertices varies. In hyperspectral image processing

they are identified with endmember materials in the linear mixing model. In content based image retrieval, they correspond to a base of shapes.

We present a computational procedure for the induction of the vertices of a convex region covering most of the data points. This procedure makes profit of the selective noise sensitivity of the Associative Morphological Memories (AMM) to detect the morphological independence conditions that are a necessary condition of the convex region vertices. In its actual implementation it works in a single pass over the data sample. The procedure is unsupervised and does not need the explicit setting of the number of region vertices searched for, although it is determined indirectly by the setting of the noise filtering parameter α. Lower values allow for higher number of vertices. By construction the maximum number of vertices is two times the dimension of the data space: only two vertices are allowed at most in each subspace spanned by each dimension unit vector.

The Associative Morphological Memories [15], [16], [17] are the morphological counterpart of the well known Hopfield Associative Memories [5]. AMM's are constructed as correlation matrices computed by either Min or Max matrix product. Dual constructions can be made using the dual Min and Max operators. Recently, [20] has shown the generalization of binary AMM's based on fuzzy set theory. The AMM selective sensitivity to specific types of noise (erosive and dilative noise) is of special interest to us. It was established that AMM are able to store and recall morphologically strongly independent sets of patterns. The notion of morphological independence and morphological strong independence was introduced in [17] to study the construction of AMM robust to general noise. When the input pattern is morphologically independent of the stored patterns, the result of recall is a morphological polynomial on the stored patterns [19]. We construct the erosive and dilative memories to store the patterns. Any input patters whose recalled output corresponds to one of the stored patterns in both kind of memories lies inside the convex region already defined by the stored patterns. Otherwise the pattern is a new vertex of the convex region enclosing the data. The data patterns are filtered dilatively and erosively before being binarized to construct and test the AMM's.

The first application of our approach is the unsupervised analysis of hyperspectral images. Supervised analysis and classification of hyperspectral remote sensing data main drawback is the difficulty in obtaining labeled sample data. The scarcity of ground truth data has been recognized and specific training strategies have been devised to cope with this handicap [21, 22]. From our point of view, the emphasis must be in the unsupervised analysis and segmentation of the hyperspectral data to obtain salient image regions that may deserve further analysis and search for labeled data. Most unsupervised segmentation attempts have been based on clustering algorithms, including artificial neural networks derived from the SOM paradigm [24]. These approaches either ignore small features of the data or must be over-parameterized to associate any representative to them. Therefore, it is difficult for them to detect and isolate small regions of the image with salient spectral features. In essence, SOM related algorithms are searching for data averages, while salient feature vectors are outliers of the data cloud. The approach we favor is that of linear filtering for target detection [10] and the "spectral unmixing" [9] model.

We assume a linear mixing model, in which several basic materials (endmembers) are combined according to some abundance coefficients at each image pixel. Taking its spatial distribution, the abundance coefficients may be visualized as abundance images, which give a description of material distribution in the space. The computation of the abundance coefficients given a pixel spectra and a set of endmembers is the unmixing procedure. If the endmembers are known a priori, the unmixing procedure is equivalent to the parallel detection of the spectral features represented by the endmembers (i.e.: materials). If the endmembers are a priori unknown, but induced from the image data, the procedure may be interpreted as an unsupervised segmentation of the image. We test our approach against Convex Cone Analysis (CCA) and ICA in this problem.

The other application of interest is the content based image retrieval (CBIR) of shape images [23]. The CBIR problem is that of finding within a set of images the ones more similar to a given one. The role of the feature extraction algorithm is to map the images to low dimensional vectors whose topology reflects the visual similarity between shapes. The shape of the objects is described by the distribution of a set of significative shape points [1]. The PCA and ICA have been used to perform dimension reduction on this problem, before applying classifiers (like the k-NN or naive bayes) to shape recognition. In this paper we will apply our AMM based approach to the shapes in the Squid System database of fish boundaries [11] in a simple CBIR experiment. The validation of the approach can not be based in a quantitative measure, nevertheless the visual results are very positive.

2 Linear mixing model and linear feature extraction

The linear mixing model [9] can be expressed as follows:

$$\mathbf{x} = \sum_{i=1}^{M} a_i \mathbf{s}_i + \mathbf{w} = \mathbf{S}\mathbf{a} + \mathbf{w}, \tag{1}$$

where $\mathbf{x}$ is the d-dimension pattern vector, $\mathbf{S}$ is the $d \times M$ matrix whose columns are the d-dimension vertices of the convex region covering the data $\mathbf{s}_i, i = 1, .., M$, $\mathbf{a}$ is the M-dimension fractional abundance vector, and $\mathbf{w}$ is the d-dimension additive observation noise vector. The linear mixing model is subjected to two constraints on the abundance coefficients. First, to be physically meaningful, all abundance coefficients must be non-negative $a_i \geq 0, i = 1, .., M$. Second, to account for the entire composition, they must be fully additive $\sum_{i=1}^{M} a_i = 1$. Once the convex region vertices have been determined the unmixing is the computation of the matrix inversion that gives the coordinates of the point inside the convex region. The simplest approach is the unconstrained least squared error estimation given by:

$$\hat{\mathbf{a}} = \left(\mathbf{S}^T\mathbf{S}\right)^{-1}\mathbf{S}^T\mathbf{x}. \tag{2}$$

The coefficients that result from this computation do not necessarily fulfill the non-negativity and full additivity conditions. It is possible to enforce each condi-

tion separately, but rather difficult to enforce both simultaneously [9]. The added complexity may render the whole approach rather impractical, therefore we will use unconstrained estimation (2) to compute the abundance images. In the setting of hyperspectral image processing, the convex coordinates are interpreted as the fractional abundance coefficients of the endmember materials in the scene pixel. In the setting of shape retrieval, the abundance coefficients become the feature vector, and the similarity measure is the Euclidean distance. In the following we present the ICA and CCA methods that will be applied in hyperspectral image processing to compare with our approach. ICA as a linear feature extraction and CCA as an alternative method for endmember induction for linear unmixing.

2.1 Independent Component Analysis (ICA)

The Independent Component Analysis (ICA) [7] assumes that the data is a linear combination of nongaussian, mutually independent latent variables with an unknown mixing matix. The ICA reveals the hidden independent sources and the mixing matrix. That is, given a set of observations represented by a D dimensional vector $\mathbf{x}$, ICA assumes a generative model $\mathbf{x} = \mathbf{A}\mathbf{s}$, where $\mathbf{s}$ is the M dimensional vector of independent sources and $\mathbf{A}$ is the $D \times M$ unknown basis matrix. The ICA searches for the linear transformation of the data $\mathbf{W}$, such that the projected variables $\mathbf{W}\mathbf{x} = \mathbf{s}$ are as independent as possible. It has been shown that the model is completely identifiable if the sources are statistically independent and at least $M-1$ of them are non gaussian. If the sources are gaussian the ICA transformation could be estimated up to an orthogonal transformation. Estimation of mixing and unmixing matrices can be done maximizing diverse objective functions, among them the non gaussianity of the sources and the likelihood of the sample. We have used the FastICA [6] algorithm available at http://www.cis.hut. /projects/ica/fastica. We have applied it to the abundance computation in hyperspectral images. To this end we did reshape the hyperspectral images so that each band becomes a data vector. The endmembers searched for are the columns of the estimated mixing matrix $\mathbf{A}$, and the estimated abundance images are the independent sources $\mathbf{s}$. Obviously, the number of independent sources M searched for is the number of endmembers, and D is the number of spectral bands.

2.2 The Convex Cone Analysis (CCA)

The CCA was proposed by [8]. The basic idea is that after PCA of the spectral correlation matrix, the data falls in a cone shaped region in the positive subspace centered in the first eigenvector. Given the $N \times M \times D$ hyperspectral image, it is reorganized as a $NM \times D$ matrix $\mathbf{S}$. The spectral correlation matrix is computed as $\mathbf{C} = \mathbf{S}^T\mathbf{S}$. Let it be $\mathbf{C} = \mathbf{P}\mathbf{L}\mathbf{P}^T$ the PCA decomposition of the correlation matrix, select the first c eigenvectors $[\mathbf{p}_1, .., \mathbf{p}_c] = \mathbf{P}_c$ and search for the boundaries of the convex region characterized by $\mathbf{x} = \mathbf{p}_1 + a_1\mathbf{p}_2 + .. + \mathbf{a}_{c-1}\mathbf{p}_c \geq \mathbf{0}$. The vertices of this region are the points with exactly $c-1$ zero components. The CCA algorithm searches among all the $\binom{b}{c-1}$ possible combinations of eigenvectors performing the following test. Let it be $\left[\mathbf{p}\left(\gamma_1\right), .., \mathbf{p}\left(\gamma_{c-1}\right)\right] = \mathbf{P}'$ the selected set of eigenvectors.

Solve the set of equations $\mathbf{P}'\mathbf{a} = \mathbf{0}$ and compute $\mathbf{x} = \mathbf{P}_c\mathbf{a}$. If $\mathbf{x}$ has exactly $c-1$ zero components it is a vertex of the convex region data. In practice, each component is tested against a threshold. However, as the combinatorial space grows the problem becomes intractable. We implemented an straightforward random search. Application of more sophisticated random search algorithms like genetic algorithms may be of interest for large problems. The CCA algorithm provides the endmembers that may be used to compute the abundance images.

3 Associative Morphological Memories

The work on Associative Morphological Memories stems from the consideration of an algebraic lattice structure $(\mathbb{R}, \vee, \wedge, +)$ as the alternative to the algebraic $(\mathbb{R}, +, \cdot)$ framework for the definition of Neural Networks computation [15] [16]. The operators $\vee$ and $\wedge$ denote, respectively, the discrete max and min operators (resp. sup and inf in a continuous setting), which correspond to the morphological dilation and erosion operators, respectively. Given a set of input/output pairs of pattern $(X, Y) = \left\{\left(\mathbf{x}^\xi, \mathbf{y}^\xi\right); \xi = 1, .., k\right\}$, an heteroassociative neural network based on the pattern's cross correlation [5] is built up as $W = \sum_\xi \mathbf{y}^\xi \cdot \left(\mathbf{x}^\xi\right)'$. Mimicking this construction procedure [15], [16] propose the following constructions of Heteroassociative Morphological Memories (HMM's):

$$W_{XY} = \bigwedge_{\xi=1}^{k} \left[\mathbf{y}^\xi \times \left(-\mathbf{x}^\xi\right)'\right] \text{ and } M_{XY} = \bigvee_{\xi=1}^{k} \left[\mathbf{y}^\xi \times \left(-\mathbf{x}^\xi\right)'\right], \tag{3}$$

where $\times$ is any of the $\boxtimes^\vee$ or $\boxtimes^\wedge$ operators. Here $\boxtimes^\vee$ and $\boxtimes^\wedge$ denote the max and min matrix product, respectively defined as follows:

$$C = A \boxtimes^\vee B = [c_{ij}] \Leftrightarrow c_{ij} = \bigvee_{k=1..n} \{a_{ik} + b_{kj}\}, \tag{4}$$

$$C = A \boxtimes^\wedge B = [c_{ij}] \Leftrightarrow c_{ij} = \bigwedge_{k=1..n} \{a_{ik} + b_{kj}\}. \tag{5}$$

If $X = Y$ then the HMM memories are Autoassociative Morphological Memories (AMM). Conditions of perfect recall by the HMM's and AMM's of the stored patterns are proved in [15],[16]. In the continuous case, the AMM's are able to store and recall any set of patterns:

$$W_{XX} \boxtimes^\vee X = X = M_{XX} \boxtimes^\wedge X, \tag{6}$$

for any X.

These results hold when we try to recover the output patterns from the noise-free input pattern. Let it be $\tilde{\mathbf{x}}^\gamma$ a noisy version of $\mathbf{x}^\gamma$. If $\tilde{\mathbf{x}}^\gamma \cdot \mathbf{x}^\gamma$ then $\tilde{\mathbf{x}}^\gamma$ is an eroded version of $\mathbf{x}^\gamma$, alternatively we say that $\tilde{\mathbf{x}}^\gamma$ is corrupted by erosive noise. If $\tilde{\mathbf{x}}^\gamma \geq \mathbf{x}^\gamma$ then $\tilde{\mathbf{x}}^\gamma$ is a dilated version of $\mathbf{x}^\gamma$, alternatively we say that $\tilde{\mathbf{x}}^\gamma$ is corrupted by dilative noise.

Morphological memories are selectively sensitive to these kinds of noise. The conditions of *robust* perfect recall are proven in [15], [16]. Here we will remember them for the sake of the reader, because they are on the basis of the proposed algorithm. Given patterns X, the equality

$$W_{XX} \mathbin{\mathbb{V}} \widetilde{\mathsf{x}}^\gamma = \mathsf{x}^\gamma \tag{7}$$

holds when the noise affecting the pattern is erosive $\widetilde{\mathsf{x}}^\gamma \cdot \mathsf{x}^\gamma$ and the following relation holds:

$$\forall i \exists j_i; \widetilde{x}_{j_i}^\gamma = x_{j_i}^\gamma \vee \left(\bigvee_{\xi \neq \gamma} \left(x_i^\gamma - x_i^\xi + x_{j_i}^\xi \right) \right). \tag{8}$$

Similarly, the equality

$$M_{XY} \mathbin{\mathbb{\Lambda}} \widetilde{\mathsf{x}}^\gamma = \mathsf{x}^\gamma \tag{9}$$

holds when the noise affecting the pattern is dilative $\widetilde{\mathsf{x}}^\gamma \geq \mathsf{x}^\gamma$ and the following relation holds:

$$\forall i \exists j_i; \widetilde{x}_{j_i}^\gamma = x_{j_i}^\gamma \wedge \left(\bigwedge_{\xi \neq \gamma} \left(x_i^\gamma - x_i^\xi + x_{j_i}^\xi \right) \right). \tag{10}$$

Therefore, the AMM will fail to recall the pattern if the noise is a mixture of erosive and dilative noise.

To obtain general noise robustness [15], [17], [19] proposed the kernel method. Related to the construction of the kernels, [17] introduced the notion of morphological independence. Here we distinguish erosive and dilative versions of this definition: Given a set of pattern vectors $X = \left(\mathsf{x}^1, ..., \mathsf{x}^k\right)$, a pattern vector y is said to be morphologically independent of X in the erosive sense if $\mathsf{y} \not\leq \mathsf{x}^\gamma; \gamma = \{1, .., k\}$, and morphologically independent of X in the dilative sense if $\mathsf{y} \not\geq \mathsf{x}^\gamma; \gamma = \{1, .., k\}$. The set of pattern vectors X is said to be morphologically independent in either sense when all the patterns are morphologically independent of the remaining patterns in the set. For the current application we want to use AMM as detectors of the set extreme points, to obtain a rough approximation of the minimal simplex that covers the data points. We note that given a set of pattern vectors $X = \left(\mathsf{x}^1, ..., \mathsf{x}^k\right)$, and the erosive W_{XX} and dilative M_{XX} memories constructed from it, and a test pattern $\mathsf{y} \notin X$, if y is morphologically independent of X in the erosive sense, then $W_{XX} \mathbin{\mathbb{V}} \mathsf{y} \notin X$. Also, if y is morphologically independent of X in the dilative sense, then $M_{XX} \mathbin{\mathbb{\Lambda}} \mathsf{y} \notin X$. Therefore the AMM's can be used as detectors of morphological independence.

The vector patterns that we are searching for define a high dimensional box centered at the origin of the high dimensional space (the data mean is shifted to the origin). They are morphologically independent vectors both in the erosive and dilative senses, and they enclose the remaining vectors. Working with integer valued vectors, given a set of pattern vectors $X = \left(\mathsf{x}^1, ..., \mathsf{x}^k\right)$ and the erosive W_{XX} and dilative M_{XX} memories constructed from it, if a test pattern $\mathsf{y} < \mathsf{x}^\gamma$

for some $\gamma \in \{1,..,k\}$ then $W_{XX} \not\vee \mathbf{y} \notin X$. Also, if the test pattern $\mathbf{y} > \mathbf{x}^{\gamma}$ for some $\gamma \in \{1,..,k\}$ then $M_{XX} \not\wedge \mathbf{y} \geq \notin X$. Therefore, working with integer valued patterns the AMM will be useless for the detection of morphologically independent patterns. However, if we consider the binary vectors obtained as the sign of the vector components, then morphological independence would be detected as suggested above: The already detected endmembers are used to build the erosive and dilative AMM. If the output recalled by a new pattern does not coincide with any of the endmembers, then the new pattern is a new endmember.

4 The selection of vertices from the data

The region of the space enclosed by a set of vectors which are morphologically independent in both erosive and dilative senses simultaneously is a high dimensional box that approaches the minimal simplex enclosing the data points. Let us define $\{\mathbf{f}(i) \in \mathbb{R}^d; i = 1,..,n\}$ the high dimensional data that may be the pixels in a multispectral or hyperspectral image, or selected points in shape representation, μ and σ the vector mean and standard deviations computed over the data sample, α the noise correction factor and E the set of already discovered vertices. The noise amplitude in (1) is estimated as σ, the patterns are corrected by the addition and subtraction of $\alpha\sigma$, before being presented to the AMM's. The gain parameter α controls the amount of flexibility in the discovering of new endmembers. Let us denote by the expression $\mathbf{x} > \mathbf{0}$ the construction of the binary vector $(\{b_i = 1 \text{ if } x_i > 0; b_i = 0 \text{ if } x_i \cdot \ 0\}; i = 1,..,n)$.

The steps in the procedure are the following:

1. Shift the data sample to zero mean
   $\{\mathbf{f}^c(i) = \mathbf{f}(i) - \mu; i = 1,..,n\}$.
2. Initialize the set of vertices $E = \{\mathbf{e}_1\}$ with a randomly picked sample. Initialize the set of morphologically independent binary signatures $X = \{\mathbf{x}_1\} = \left\{\left(e_k^1 > 0; k = 1,..,d\right)\right\}$
3. Construct the AMM's based on the morphologically independent binary signatures: M_{XX} and W_{XX}.
4. For each pixel $\mathbf{f}^c(i)$
   (a) compute the noise corrections sign vectors $\mathbf{f}^+(i) = (\mathbf{f}^c(i) + \alpha\sigma > \mathbf{0})$ and $\mathbf{f}^-(i) = (\mathbf{f}^c(i) - \alpha\sigma > \mathbf{0})$
   (b) compute $y^+ = M_{XX} \not\wedge \mathbf{f}^+(i)$
   (c) compute $y^- = W_{XX} \not\vee \mathbf{f}^-(i)$
   (d) if $y^+ \notin X$ or $y^- \notin X$ then $\mathbf{f}^c(i)$ is a new vertex to be added to E, go to step 3 and resume the exploration of the data sample.
   (e) if $y^+ \in X$ and $\mathbf{f}^c(i) > \mathbf{e}_{y^+}$ the pixel spectral signature is more extreme than the stored vertex, then substitute $\mathbf{e}_{y^+}$ with $\mathbf{f}^c(i)$.

(f) if $y^- \in X$ and $\mathbf{f}^c(i) < \mathbf{e}_{y^-}$ the new data point is more extreme than the stored vertex, then substitute $\mathbf{e}_{y^-}$ with $\mathbf{f}^c(i)$.

5. The final set of vertices is the set of original data vectors $\mathbf{f}(i)$ of the sign vectors selected as members of E.

5 Experimental results

We will first present the results on the unsupervised segmentation of hyperspectral images, where we compare our approach with the ICA and CCA. The experiment was done on a synthetic image allowing precise quantitative validation of the results. Finally we discuss some results on the application of our approach to the shape similarity computation on the fish contours database.

5.1 The experimental hyperspectral image

In previous works [3, 4] we have presented results on a classical hyperspectral image reference. Here we have made use of synthetic images to test our approach and the benchmark CCA and ICA algorithms. This allows a very precise characterization of the performances because we can compute the correlation between the ground truth abundance images and the ones induced by the algorithms. The hyperspectral image used for the experimental results reported here is generated as linear mixtures of a set of spectra (the ground truth endmembers) with synthesized abundance images. The ground truth endmembers were selected from the USGS spectral libraries corresponding to the AVIRIS flights.

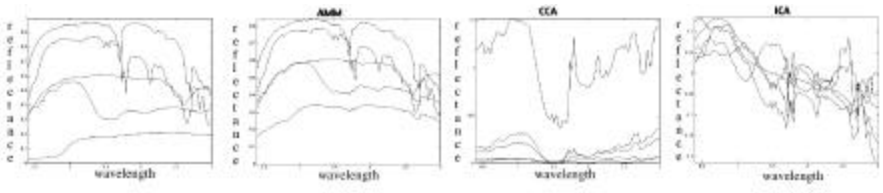

Figure 1: From left to right, plots of the ground truth endmembers extracted from the USGS library, endmembers induced from the data by our AMM approach, CCA and ICA

Figure 1 left plot shows the spectra used as endmember in the synthetic images. The synthetic ground truth abundance images were generated in a two step procedure, first we simulate each as an 2D Legendre polynomial. Legendre polynomials on 2D and 3D supports have been proposed by [18] for the modeling of illumination bias in the context of illumination inhomogeneity correction. The l-order 2D

Legendre polynomial is defined as

$$b(x,y;\{p_{ij}\}) = \sum_{i=0}^{l}\sum_{j=0}^{l-1} p_{ij} P_i(x) P_j(y) \tag{11}$$

where $P_i(x)$ refers the i-th order Legendre polynomial computed on the x axis.The $P_i(x) P_j(y)$ 2D polynomials are orthogonal and constitute a basis of the space of images.

To ensure that there are regions of almost pure endmembers we selected for each pixel the abundance coefficient with the greater value and we normalize the remaining to ensure that the abundance coefficients in this pixel sum up to one. It can be appreciated on the abundance images that each endmember has several region of almost pure pixels, viewed as brighter regions in the images. Image size is 64×64 pixels of 224 spectral bands each. The left column in figure 2 presents the ground truth abundance images of the 5 endmember hyperspectral image, which were generated using Legendre polynomials of order 10 and 11. Note that the last one which appears black, has a white pixel in the lower right corner. This very small feature is a rather difficult target for detection.

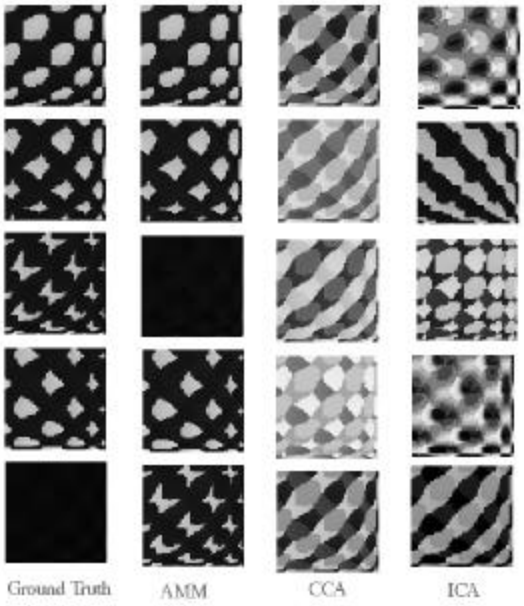

Figure 2: Abundance images generated with Legendre polynomials of order 10 and 11, used to synthesize a 5 endmember hyperspectral image, and the abundance images induced by the AMMs, ICA, CCA from the data

An additional reason to choose the Legendre polynomials to synthesize the ground truth abundance images is that the distribution of the pixel intensities is

non gaussian. The histograms of the ground truth abundance images in figure 3 show a strong departure from gaussianity. Therefore ICA is in the best of the scenarios for its application.

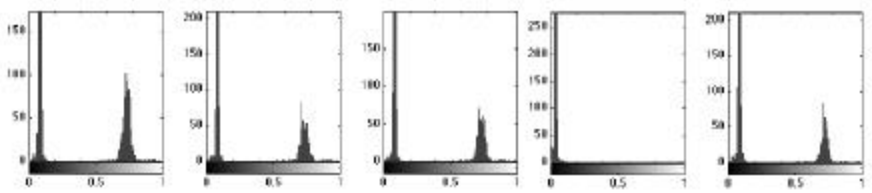

Figure 3: Histograms of the ground truth abundance images.

5.2 Experimental results on the hyperspectral image

When applying the ICA and CCA methods we have set the desired number of endmembers to the exact number of ground truth endmembers. Our AMM approach needed the setting of the noise gain parameter α. After some trials, we set $\alpha = 0.3$ for this synthetic hyperespectral image. Values in the range $0.3 < \alpha < 1.0$ produced systematically the detection of 4 endmembers, increasing the value gave lesser endmembers until only one could be detected. The experiment consisted on the computation of the endmembers and abundance images induced by each method and the quality measure was the correlation between the induced and ground truth images. The induced images were not ordered, therefore we considered the maximum correlation for each induced abundance image with anyone of the ground truth abundance images, and we plotted them ordered in figure 4. It can be appreciated that our approach "discovered" the ground truth abundances almost perfectly. It must be said that instances of the algorithm that found less endmembers produced also high correlation values. Surprisingly, CCA results are better than those of ICA despite the careful choice of the non gaussian sources. The visual results that would correspond to the unsupervised segmentation of the image are presented in figure 2. It is easy to spot the correspondence of each AMM induced abundance image with the ground truth ones. It can also be appreciated that ICA and CCA results appear to be combinations of the ground truth. Some of the abundance images of the ICA were equalized because they were almost white and did not appear visible in the figure. The induced endmembers were plotted in figure 1 along with the ground truth ones. Again our approach extracts spectra from the image which are close to the ground truth, while both CCA and ICA equivalents are rather arbitrary in shape.

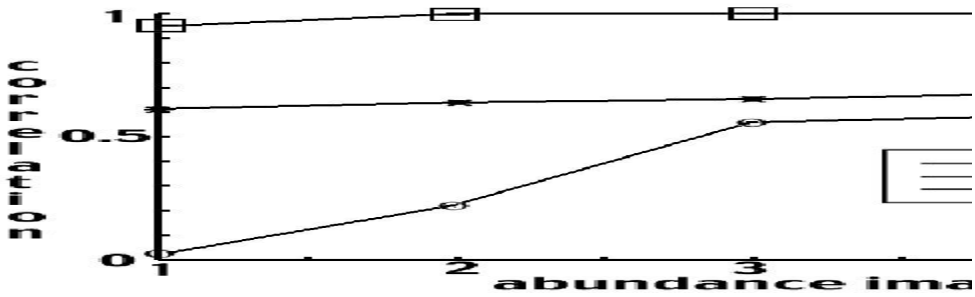

Figure 4: Correlation between the induced abundance images and the ground truth synthetic abundance images (maximum correlation sorted in ascending order)

5.3 Results of the CIBIR experiment

In order to apply our AMM based approach to the shapes in the Squid System database of fish boundaries [11] we had to preprocess them and to reduce them to a fixed number of points. We performed a straightforward average smoothing on the Euclidean coordinates taken as separate functions. On the smoothed contours we selected the 200 points with the higher absolute value of the second derivative in either axis. Then we shifted the centroid of the shape to the origin and we normalize the coordinates to a maximum value of 1. (Not a norm normalization). We computed the polar coordinates of the normalized shapes and take as our data sample vectors the plot of the magnitude starting with the leftmost point in the normalized shape. It is important to note that we did not register the shapes to have a standard orientation, we taken them as such from the original database. From then we obtained a set of 25 extreme shapes from the application of the AMM method presented in section 4. For lack of space we do not reproduce them, but instead we present in figure 5 the morphing between two of these extreme shapes that happens when we vary a mixing parameter. From left to right, top to bottom the shapes correspond to the ones that lie in a segment of a hiperline connecting the shapes in the upper left and lower right positions. All the images have a feasible appearance, which demonstrates that our characterization of the shape space is somehow complete in the sense that the detected extreme shapes define a region of well-defined shapes in a very high dimensional space. Note also that the orientation of both extreme shapes is quite different.

As a second test of the power of the representation obtained, we computed the convex coordinates of each shape in the database on the basis of selected extreme shapes. Then we perform the search of the most similar shapes to a given one according to the Euclidean distance between their feature vectors (the convex coordinates). Figure 6 shows three of these queries into the database. The smaller shapes to the right of the queries are the most similar ones in the database. It can be appreciate that orientation is preserved in this process and that visual similitude of the recalled shapes is very high. It is not possible to give quantitative measures

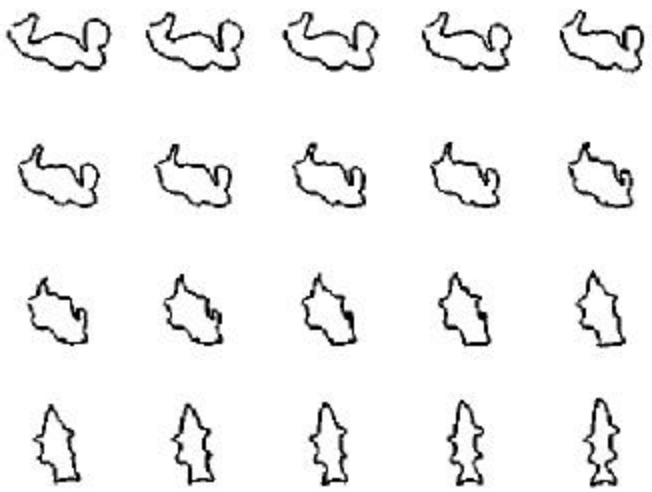

Figure 5: Morphing from one extreme shape to another varying the degree of mixing from 0 to 1

of the recall because the exact distribution of species, families and genders on the database is unknown, as well as the distribution of orientations.

6 Conclusions and Further Work

The argument of this paper is twofold. First we claim that we can use as features the convex coordinates of the data points based on the vertices of a convex region covering the data. Second we did apply AMM as a tool to detect morphologically independent vectors in the data sample, assuming that morphological independence is a necessary condition for the vertices of a convex region. The application of this ideas to the unsupervised segmentation of hyperspectral images and to the search for similar shapes in a fish contour database shows both the adequacy of convex coordinates as data features and the superiority of our approach to other endmember induction algorithms (CCA) and linear transforms (ICA). Future work will be addressed to continue the experimentation on hyperspectral images, both synthetic and real, and benchmarking against other algorithms. On the shape similarity experiments we plan to apply our approach to shape databases conveniently labeled so that classification results with a standard classifier (k-NN or naive bayes) could be used as validation measures.

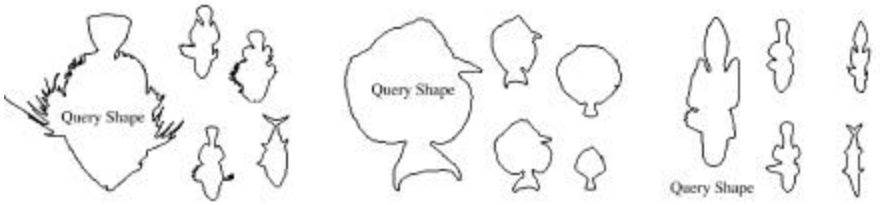

Figure 6: Some instances of querying the collection of shapes using as features the ones derived from testing morphological independence with the AMM.

Acknowledgment

The authors received support from projects of the Ministerio de Ciencia y Tecnologia TIC2000-0739-C04-02 and TIC2000-0376-P4-04

References

[1] Cootes T.F., C.J. Taylor, D.H. Cooper, J. Graham, (1995) Active shape models- their training and application, Comp. Vision and Im. Unders. 61:38-59

[2] Fukunaga K., Introduction to statistical pattern recognition, Academic Press, Boston, MA 1990

[3] Graña M., J. Gallego, Associative Mophological Memories for endmember induction, Proc. IGARSS'2003, Tolouse, France.

[4] Graña M., P. Sussner, G. Ritter, Associative Morphological Memories for Endmember Determination in Spectral Unmixing, Proc. FUZZ-IEEE'03

[5] Hopfield J.J., (1982) Neural networks and physical systems with emergent collective computational abilities, Proc. Nat. Acad. Sciences, vol. 79, pp.2554-2558,

[6] Hyvarynën A., E. Oja A fast fixed-point algorithm for independen component analysis, Neural Comp. 9:1483-1492, 1999

[7] Hyvarynën A., J. Karhunen, E. Oja, Independent Component Analysis, John Wiley & Sons, New York, 2001

[8] Ifarraguerri A., C.-I Chang, (1999) Multispectral and Hyperspectral Image Analysis with Convex Cones, IEEE Trans. Geos. Rem. Sensing, 37(2):756-770

[9] Keshava N., J.F. Mustard Spectral unimixing, IEEE Signal Proc. Mag. 19(1) pp:44-57 (2002)

[10] Manolakis D., G. Shaw Detection algorithms for hyperspectral imaging applications, IEEE Signal Proc. Mag. 19(1) pp:29-43 (2002)

[11] Mokhtarian, F. Abbasi S. and Kittler J. Robust and Efficient Shape Indexing through Curvature Scale Space in Proceedings of the sixth British Machine Vision Conference, BMVC'96. Edinburgh, 10-12 September 1996,pp 53-62.

[12] Plaza A., P. Martinez, R. Perez, J. Plaza, Spatial Spatial/Spectral Endmember Extraction by Multidimensional Morphological Operations, IEEE Trans. Geoscience Remote Sensing, 40(9) pp. 2025-2041

[13] Raducanu B., M. Graña, X. Albizuri (2003) Morphological scale spaces and associative morphological memories: results on robustness and practical applications, J. Math. Imaging and Vision 19(2):113-122

[14] Rand R.S., D.M.Keenan (2001) A Spectral Mixture Process Conditioned by Gibbs-Based Partitioning, IEEE Trans. Geos. Rem. Sensing, 39(7):1421-1434

[15] Ritter G. X., J. L. Diaz-de-Leon, P. Sussner. (1999) Morphological bidirectional associative memories. Neural Networks, Volume 12, pages 851-867,

[16] Ritter G. X., P. Sussner, J. L. Diaz-de-Leon. (1998) Morphological associative memories. IEEE Trans. on Neural Networks, 9(2):281-292,

[17] Ritter G.X., G. Urcid, L. Iancu, (2003) Reconstruction of patterns from moisy inputs using morphological associative memories, J. Math. Imaging and Vision 19(2):95-112

[18] Styner M., G. Gerig, C. Brechbuhler, G. Szekely (2000) Parametric estimate of intensity inhomogeneities applied to MRI. IEEE Trans. Med. Imaging , 19(3), pp. 153-165.

[19] Sussner P., (2001) Observations on Morphological Associative Memories and the Kernel Method, Proc. IJCNN'2001, Washington DC, July

[20] Sussner P., (2003) Generalizing operations of binary autoassociative morphological memories using fuzzy set theory, J. Math. Imaging and Vision 19(2):81-94

[21] Tadjudin, S. and D. Landgrebe,(1999) Covariance Estimation with Limited Training Samples, IEEE Trans. Geos. Rem. Sensing, 37(4):2113-2118,

[22] Tadjudin, S. and D. Landgrebe,(2000) Robust parameter estimation for mixture model, IEEE Trans. Geos. Rem. Sensing, 38(1):439

[23] Veltkamp R.C., M. Hagedoorn (2001) State of the art in shape matching, in M.S. Lew (ed) Principles of visual information retrieval, Berlin, Springer Verlag

[24] Villman T., Merenyi E. Hammer B. (2003) Neural Maps in remote sensing image analysis, Neural Networks, 16:389-403